Brain-state dependent astrocytic Ca^{2+} signals are coupled to both positive and negative BOLD-fMRI signals

Maosen Wang[a,b], Yi He[a,b], Terrence J. Sejnowski[c,d,1], and Xin Yu[a,1]

[a]Translational Neuroimaging and Neural Control Group, High Field Magnetic Resonance Department, Max Planck Institute for Biological Cybernetics, 72076 Tuebingen, Germany; [b]Graduate Training Centre of Neuroscience, International Max Planck Research School, University of Tuebingen, 72074 Tuebingen, Germany; [c]Howard Hughes Medical Institute, Computational Neurobiology Laboratory, Salk Institute for Biological Studies, La Jolla, CA 92037; and [d]Division of Biological Sciences, University of California, San Diego, La Jolla, CA 92093

Contributed by Terrence J. Sejnowski, January 5, 2018 (sent for review June 30, 2017; reviewed by Emery N. Brown and Eric A. Newman)

Astrocytic Ca^{2+}-mediated gliovascular interactions regulate the neurovascular network in situ and in vivo. However, it is difficult to measure directly both the astrocytic activity and fMRI to relate the various forms of blood-oxygen-level-dependent (BOLD) signaling to brain states under normal and pathological conditions. In this study, fMRI and GCaMP-mediated Ca^{2+} optical fiber recordings revealed distinct evoked astrocytic Ca^{2+} signals that were coupled with positive BOLD signals and intrinsic astrocytic Ca^{2+} signals that were coupled with negative BOLD signals. Both evoked and intrinsic astrocytic calcium signal could occur concurrently or respectively during stimulation. The intrinsic astrocytic calcium signal can be detected globally in multiple cortical sites in contrast to the evoked astrocytic calcium signal only detected at the activated cortical region. Unlike propagating Ca^{2+} waves in spreading depolarization/depression, the intrinsic Ca^{2+} spikes occurred simultaneously in both hemispheres and were initiated upon the activation of the central thalamus and midbrain reticular formation. The occurrence of the intrinsic astrocytic calcium signal is strongly coincident with an increased EEG power level of the brain resting-state fluctuation. These results demonstrate highly correlated astrocytic Ca^{2+} spikes with bidirectional fMRI signals based on the thalamic regulation of cortical states, depicting a brain-state dependency of both astrocytic Ca^{2+} and BOLD fMRI signals.

BOLD-fMRI | astrocyte | calcium | brain states | glia-vascular coupling

The blood-oxygen-level-dependent (BOLD) signal is used in many fMRI studies as a surrogate for brain activity, but the link between the two signals is indirect, which makes the interpretation of BOLD signals problematic. The neurovascular coupling that underpins functional MRI (fMRI) brain mapping (1) has been characterized by simultaneous intracortical recordings and fMRI (2). Among the neurovascular signaling events, it remains ambiguous how gliovascular interactions, especially that mediated by the astrocytic Ca^{2+} signal, are involved in the neurovascular network (3–6). Astrocytic Ca^{2+} signals in both in situ and in vivo environments can occur in coordination with, or independently of, each other, suggesting specific and variable coupling mechanisms (5, 7–13). It is difficult to directly measure astrocytic activity, which may vary according to different normal brain states and pathological conditions (14–17), while simultaneously utilizing fMRI.

It is possible to use genetically encoded Ca^{2+} indictors (GECIs, e.g., GCaMP) to acquire cell type-specific Ca^{2+} signals via optical fiber, which can be measured during fMRI imaging without radiofrequency and magnetic gradient-switch induced interference (2, 18–21). In particular, GCaMP6f shows fast Ca^{2+} binding kinetics and high sensitivity comparable to the Ca^{2+}-sensitive dyes, such as Oregon Green BAPTA-1 (OGB-1) (18, 20). Besides two-photon microscopy (22) or wide-field calcium imaging (23), the Ca^{2+}-sensitive dye and GCaMP-mediated Ca^{2+} signal can be directly recorded using optical fiber implanted into animal brains (19, 24, 25). The fMRI signal may be simultaneously acquired with the Ca^{2+} signal from neurons or astrocytes specifically loaded with Ca^{2+}-sensitive dyes (19). These studies show that it is feasible to monitor the many possible ways that astrocytes mediate BOLD signals through specific neurovascular coupling events.

We have observed the expected positive correlation between the evoked neuronal/astrocytic Ca^{2+} signals and BOLD fMRI signal in activated cortical areas; however, an unexpected intrinsic astrocytic Ca^{2+} signal showing negative correlation with both neuronal and fMRI signals can occur concurrently with the evoked neurovascular coupling events. In contrast to the spreading depolarization/depression-based traveling Ca^{2+} waves in the brain (26, 27), this intrinsic astrocytic Ca^{2+} signal represents distinct spatiotemporal features that occur simultaneously in both hemispheres without propagation delays (28–32). The instantaneously altered brain activity that is associated with the intrinsic astrocytic Ca^{2+} signal is a unique astrocyte-mediated change in brain state (9, 33, 34).

We provide evidence that subcortical nuclei projecting to the entire cortex are responsible for regulating the astrocytic calcium-coupled bidirectional fMRI signal. By using astrocytic Ca^{2+} signal-based event-related fMRI analysis, positive BOLD signals were

Significance

The role of astrocytes on brain function is controversial in many aspects. It remains challenging to specify the in vivo functional impact of astrocytic calcium signal when mediating vasodilation/constriction at varied physiological or pathophysiological conditions. Here, we applied simultaneous fMRI and GCaMP-mediated Ca^{2+} optical fiber recording to detect distinct astrocytic Ca^{2+} signals (evoked vs. intrinsic) coupled to positive and negative blood-oxygen-level-dependent signals, respectively and concurrently, with unique spatial and temporal patterns. Not only did we demonstrate the distinct neurovascular coupling events coupled to the evoked and intrinsic astrocytic calcium signals, but also revealed the thalamic regulation mechanism underlying the astrocytic calcium-mediated brain state switch. This astrocytic-relevant regulatory mechanism could underlie numerous brain disorder and injury models relevant to gliovascular disruption.

Author contributions: T.J.S. and X.Y. designed research; M.W., Y.H., and X.Y. performed research; M.W., Y.H., and X.Y. analyzed data; and M.W., T.J.S., and X.Y. wrote the paper.

Reviewers: E.N.B., Massachusetts General Hospital; E.A.N., University of Minnesota.

The authors declare no conflict of interest.

[1]To whom correspondence may be addressed. Email: terry@salk.edu or xin.yu@tuebingen.mpg.de.

This article contains supporting information online at www.pnas.org/lookup/suppl/doi:10.1073/pnas.1711692115/-/DCSupplemental.

detected at the central and mediodorsal thalamic nuclei extending to the midbrain reticular formation, which is associated with the intrinsic astrocytic Ca^{2+} signal followed by the negative BOLD signals in the cortex. This result is consistent with a resting-state fMRI study of unanesthetized macaques, showing increased thalamic fMRI signals with widespread signal decreases in the neocortex during elevated arousal states (15). This work demonstrates that astrocytes might be involved in mediating the bidirectional fMRI signal arising from the thalamic regulation of brain states, demonstrating a way to bridge the study of brain function among the cellular, network, and systems levels.

Results

Identifying the Neurovascular Coupling Events with Simultaneous fMRI and Neuronal/Astrocytic Ca^{2+} Recordings. We recorded the cell type-specific Ca^{2+} signal simultaneously with the local field potential (LFP). GCaMP6f was expressed by viral injection into the forepaw somatosensory cortex (FP-S1) of the rat brain, specifically into neurons or astrocytes (Fig. 1*A*). The sensory-evoked Ca^{2+} signal from neurons matched well with the evoked LFP for each electrical stimulus, and the amplitude of the Ca^{2+} signal was positively correlated with that of the LFP, as shown in Fig. 1*B* and *SI Appendix*, Fig. S1. Spontaneous Ca^{2+} spikes were also detected from neurons whose amplitudes were positively correlated with those of the spontaneous LFPs (*SI Appendix*, Fig. S1 *D* and *F*). The latency of the neuronal Ca^{2+} signal reported by GCaMP6f was ~15 ms with a full width of half maximum (FWHM) of 150–200 ms (*SI Appendix*, Fig. S2*A*), similar to the kinetics of GCaMP6f-mediated Ca^{2+} signals reported previously (20, 24).

In contrast to the neuronal Ca^{2+} signal, the sensory-evoked astrocytic Ca^{2+} signal was a unitary event following a train of electrical stimuli to the forepaw (Fig. 1*B*). The latency of the astrocytic Ca^{2+} signal was 1.0–1.7 s, and the FWHM was proportional to the stimulus duration, matching the simultaneously acquired BOLD signal (*SI Appendix*, Figs. S2 *B* and C and S3). The latency detected by optical fiber could reflect fast astrocytic Ca^{2+} signals within astrocyte processes (11, 35). The spread function of the astrocytic Ca^{2+} signal is derived from the sum of individual astrocytes exposed under the tip of optical fiber, which have varied response kinetics as observed in vivo with two-photon microscopy (5, 10). These results clearly demonstrated that the GCaMP6f-mediated Ca^{2+} signal from either neurons or astrocytes is specifically detectable in vivo via optical fiber, showing distinct temporal features to sensory stimulation. It is noteworthy that the evoked fluorescent Ca^{2+} signal is independent of the hemoglobin-based intrinsic optical signal, similar to the previous fiber optic Ca^{2+} studies (details in *Materials and Methods*) (21, 25).

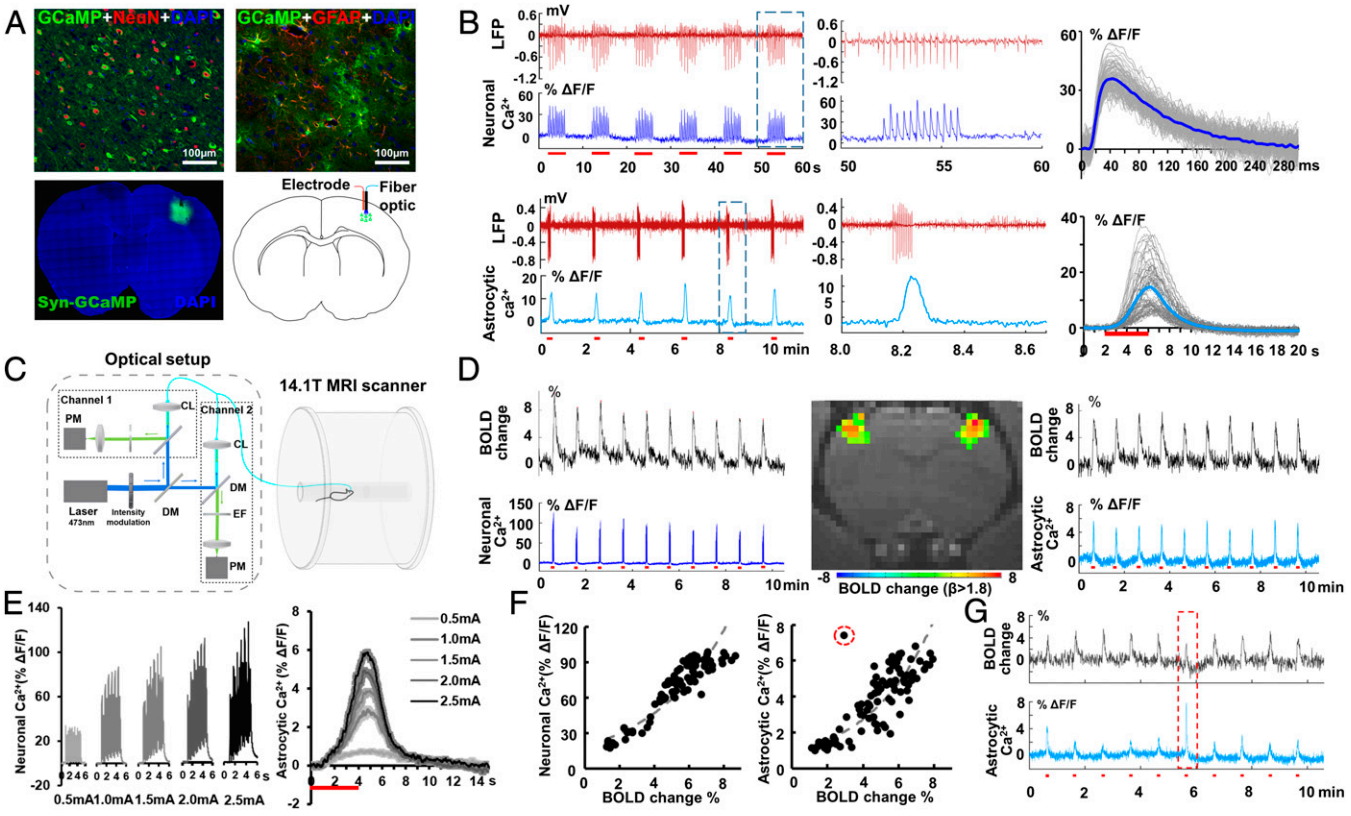

Fig. 1. Sensory-evoked neuronal/astrocytic Ca^{2+} recordings with simultaneous LFP or BOLD fMRI. (*A*) The colocalized GCaMP (green) with neurons (NeuN, red), or with astrocytes (GFAP, red). (*Lower*) Immunostaining image (*Left*) and a schematic drawing (*Right*) for simultaneous LFP and fiber-optic Ca^{2+} recording. (*B*) Simultaneous LFP (red) and Ca^{2+} signal traces (blue) from neurons or astrocytes in FP-S1 with forepaw electrical stimulation (3 Hz, 4 s, 1 mA). (*Center*) Enlarged figures of the dashed box in *Left*. (*Right*) The averaged trace of evoked Ca^{2+} signal (gray lines are individual traces from six rats). (*C*) The schematic drawing of the two-channel fiber-optic recording system with fMRI (CL, coupling lens; DM, dichroic mirror; EF, emission filter; PM, photomultiplier). (*D*) The time courses of evoked fMRI signal from bilateral FP-S1 and simultaneous neuronal (*Left*)/astrocytic (*Right*) Ca^{2+} signal (*Inset*, a representative color-coded BOLD-fMRI map at 2.0 mA). (*E*) The stimulation intensity-dependent Ca^{2+} signal from neurons or astrocytes. (*F*) The scatter plot of the evoked Ca^{2+} signal amplitude vs. simultaneous fMRI peak amplitude at different stimulation intensities (red dashed circle, outlier). (*G*) The traces of BOLD-fMRI and astrocytic Ca^{2+} signals show the outlier event (red dashed box) with increased astrocytic Ca^{2+} signal, but reduced BOLD-fMRI signal (*SI Appendix*, Table S1 shows the occurrence rate of the unexpected astrocytic event).

A two-channel fluorescent signal recording system was developed to simultaneously detect the BOLD signal and the Ca^{2+} signal from neurons and astrocytes from the forepaw somatosensory cortex of both hemispheres, respectively (Fig. 1 *C* and *D*). The neuronal and astrocytic Ca^{2+} signals were correlated with the BOLD-fMRI evoked signal across electrical stimulation intensities (Fig. 1 *E* and *F* and *SI Appendix*, Fig. S4). However, a novel event was detected in which a high-amplitude astrocytic Ca^{2+} signal was coupled with a reduced amplitude BOLD fMRI signal in a single trial-on/off block design paradigm. This outlier indicates that astrocytic Ca^{2+} signaling might play another role in neuroglial and gliovascular interaction.

We investigated the properties of the intrinsic astrocyte Ca^{2+} spikes and its relationship to the simultaneously acquired fMRI signal. In rats anesthetized with α-chloralose, intrinsic astrocytic Ca^{2+} spikes occurred simultaneously with a transient frequency shift in hypersynchronized LFP bursts (Fig. 2*A*), previously described as intermittent or continuous hypersynchrony during different EEG stages (36). During the spontaneous LFP frequency shifts, there was a transient suppression of the power spectral density [Fig. 2 *B* and *C*, nonoverlapping confidence intervals (CIs); *SI Appendix*, Table S2], as well as a decrease in the fMRI signal throughout the cortex (Fig. 2 *D* and *E*). There was a negative correlation between the resting state fMRI signal and the intrinsic astrocytic Ca^{2+} spikes (Fig. 2*D* and *SI Appendix*, Fig. S5). The astrocytic Ca^{2+} spike-triggered average of the simultaneously acquired LFP power spectral profile and fMRI signal were computed. The negative BOLD signal was much delayed (−2.64 ± 0.25 s) (Fig. 2*F*) compared with the mean onset of the astrocyte Ca^{2+} spike (−4.29 ± 1.04 s) (Fig. 2*F* and *SI Appendix*, Fig. S6, the negative value is set from the zero time at the peak of astrocytic Ca^{2+} spikes, nonoverlapping Cis; *SI Appendix*, Table S2). The mean estimated onset of LFP frequency shift (−4.77 ± 1.44 s) preceded the estimated onset of the astrocyte Ca^{2+} spike, although the difference was not statistically significant. In addition, previous studies showed that the high frequency LFP power reduction occurred earlier than the astrocytic Ca^{2+} spikes in both the cortex and hippocampus of mice anesthetized with urethane (9, 30). Thus, the intrinsic astrocytic Ca^{2+} signal elevation is possibly involved in mediating this particular neurovascular event. It is noteworthy that two-channel bilateral Ca^{2+} recording (left hemisphere, neurons; right hemisphere, astrocytes) during the resting state also shows the negative correlation of the intrinsic astrocytic Ca^{2+} spike to the neuronal Ca^{2+} transients. Power spectral analysis of the neuronal Ca^{2+} transients shows similar frequency suppression shift to that of the spontaneous LFP signal (*SI Appendix*, Fig. S7).

Elevated astrocytic Ca^{2+} signals can affect vasoconstriction or vasodilation, depending on conditions (7, 8, 12, 37), but these seldom coexist during neurovascular coupling events. Interestingly, intrinsic astrocytic Ca^{2+} spikes can occur in the FP-S1 and barrel cortex concurrently with the astrocytic Ca^{2+} signal evoked by forepaw electrical stimulation (Fig. 3 *A* and *B*). As with the spontaneous astrocytic Ca^{2+} recording during the resting state, the intrinsic astrocytic Ca^{2+} spikes during stimulation were correlated with the negative BOLD signal throughout the cortex,

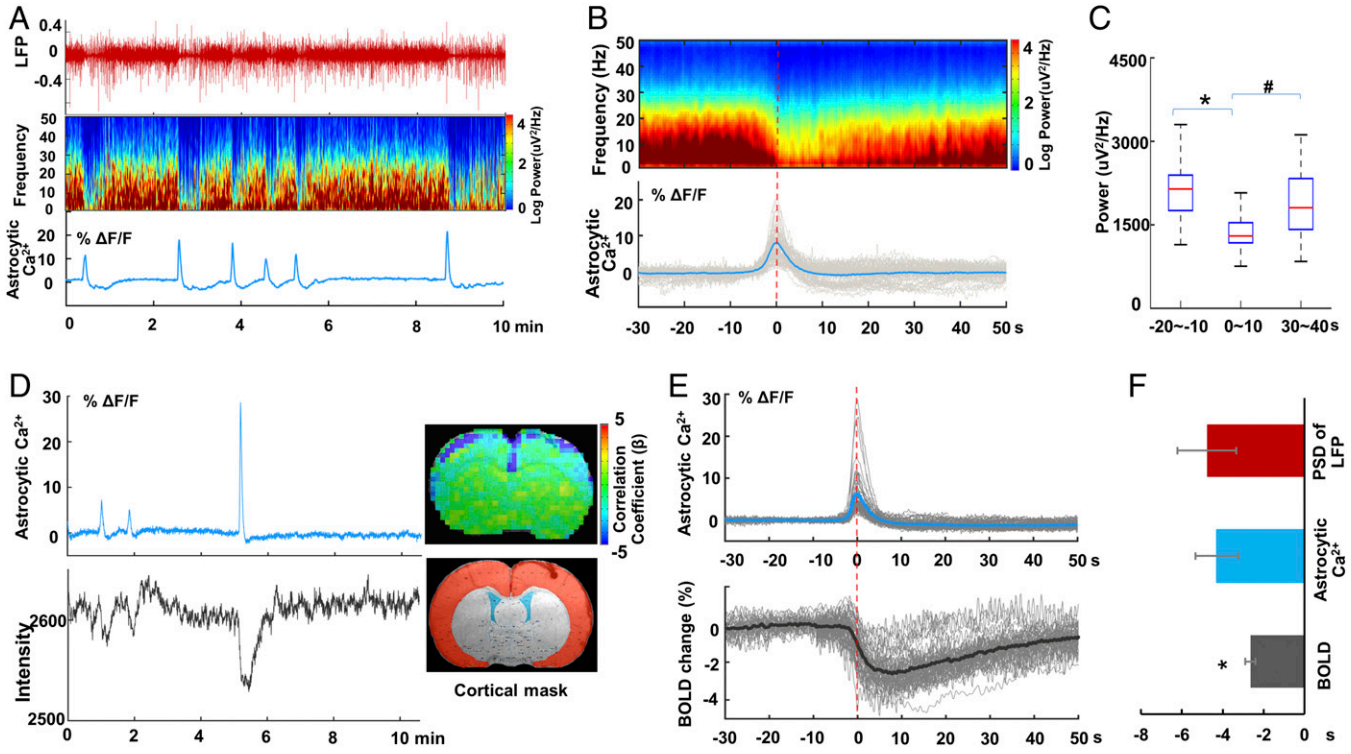

Fig. 2. Intrinsic astrocytic Ca^{2+} spikes negatively correlate with neuronal and BOLD signals. (*A*) The representative traces of the LFP (*Top*), the power spectra of LFP (*Middle*), and the intrinsic astrocytic Ca^{2+} signal (*Bottom*) in FP-S1 (1-s sliding window with 0.1-s steps, 9 tapers). (*B*) The average spectrogram of the LFP is aligned based on the simultaneously acquired peak time of the intrinsic astrocytic Ca^{2+} spikes (red dashed line as time 0). (*C*) The integrated LFP power spectral density (2 ~ 50 Hz) at different phases according to the intrinsic astrocytic Ca^{2+} spikes (*P = 9.5e-22; #P = 3.6e-11, paired t test; 54 traces of 6 rats). (*D*) The representative traces of the intrinsic astrocytic Ca^{2+} spikes and simultaneous fMRI signal acquired from the entire cortex (*Upper Inset*: color-coded negative correlation map; *Lower Inset*: ROI in red contour; details in *SI Appendix*, Fig. S5). (*E*) The averaged time course of the fMRI signal is aligned based on the simultaneous acquired peak time of the intrinsic astrocytic Ca^{2+} spikes (red dashed line as time 0, 52 traces of 6 rats). (*F*) Estimated onset times of the intrinsic astrocytic Ca^{2+} spikes, the LFP spectral power shift, and the fMRI signal reduction (time 0 at the peak time of the astrocytic Ca^{2+} spikes; one-way ANOVA followed by Tukey's multiple comparison test F = 31.94; *P = 5.1e-12, n_{LFP_Ca} = 6; n_{fMRI_Ca} = 6 rats).

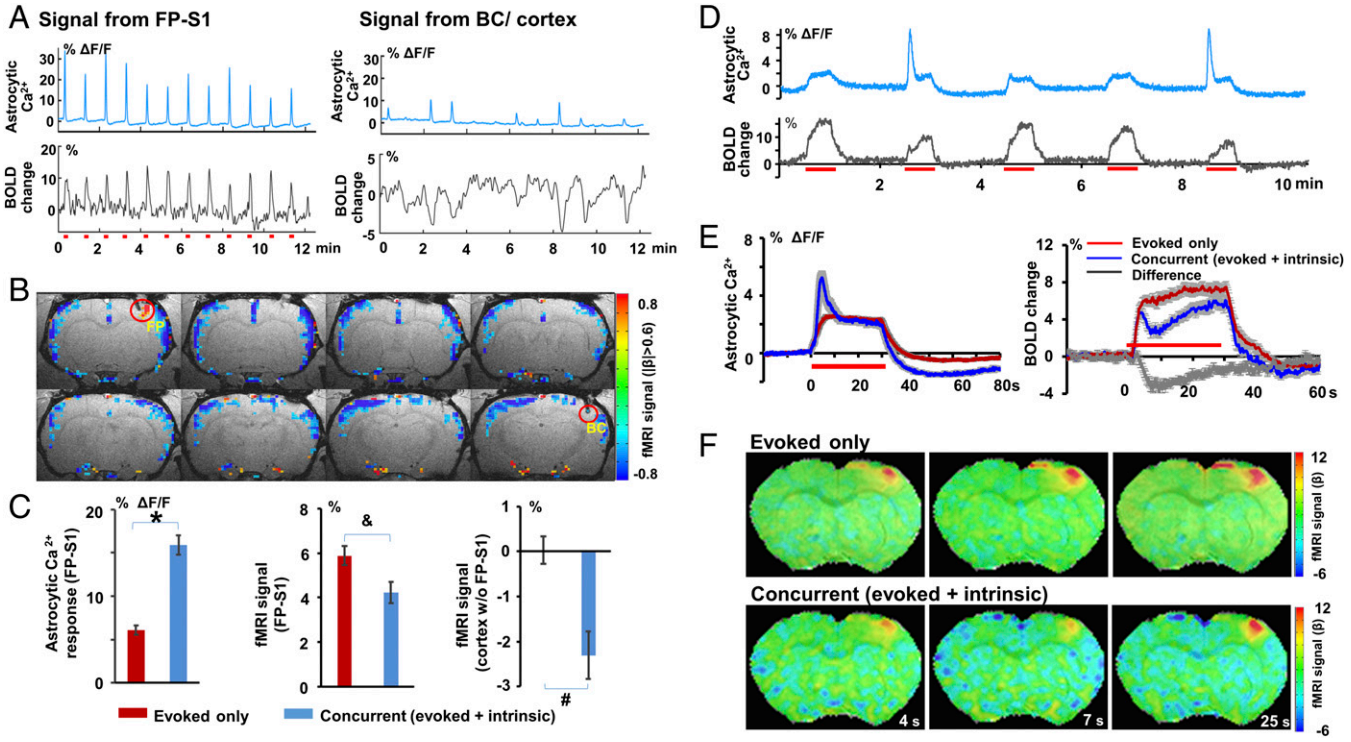

Fig. 3. Two-channel recording of the evoked and intrinsic astrocytic Ca^{2+} signal in FP-S1 and barrel cortex (BC). (*A*) The time courses of the evoked astrocytic Ca^{2+} signal and the fMRI signal from FP-S1 (*Left*) upon forepaw stimulation (3 Hz, 4 s, 1.5 mA), and the concurrent intrinsic astrocytic Ca^{2+} signal from BC and the fMRI signal from the entire cortex except FP-S1 (*Right*). (*B*) The correlation map of the fMRI signal with the intrinsic astrocytic Ca^{2+} spikes detected in BC shows negative correlation across the entire cortex except FP-S1. (*C*) The amplitude of the astrocytic Ca^{2+} signal (evoked-only) is significantly lower than that of the concurrent events in FP-S1 (*Left*, $*P = 2.0e\text{-}15$), but the fMRI signal change is significant lower in the concurrent events (*Center*, $\&P = 0.026$). The fMRI signal in the entire cortex except FP-S1 shows negative amplitude of the concurrent events, which is significantly lower than the evoked-only events (*Right*, $\#P = 2.8e\text{-}07$; evoked-only, trial # = 81; concurrent, trial # = 50, rats, $n = 7$). (*D*) The representative traces of astrocytic Ca^{2+} and corresponding fMRI signals with 30-s forepaw stimulation (evoked-only vs. concurrent: epoch 2, 5 vs. 1, 3, 4). (*E*) The mean astrocytic Ca^{2+} traces of the two events (*Left*) and the simultaneously acquired fMRI time course (*Right*; gray line, difference; evoked-only, trial # = 84 vs. concurrent, trial # = 23, mean ± SEM, rats, $n = 5$). (*F*) The representative time-lapsed BOLD-fMRI map shows FP-S1 activation during the 30-s stimulation of evoked-only and concurrent events.

with the exception of FP-S1 (Fig. 3 *B* and *C*, nonoverlapping CIs; *SI Appendix*, Table S2), where the FP-S1 BOLD signal with the concurrent (intrinsic and evoked) astrocytic Ca^{2+} signals was also lower than that with the evoked-only astrocytic Ca^{2+}signal ($P = 0.026$, Student t test two-tailed), although it was not showing nonoverlapping CIs (*SI Appendix*, Table S2). In contrast, the amplitude of the intrinsic astrocytic Ca^{2+} spike was significantly higher than the normally evoked astrocytic Ca^{2+} spike (Fig. 3*C*, nonoverlapping CIs; *SI Appendix*, Table S2). The concurrent astrocytic Ca^{2+} spiking events were better characterized in the 30-s forepaw stimulation block design experiment, which showed the intrinsic astrocytic Ca^{2+} spike superimposed on the early phase of the evoked astrocytic Ca^{2+} signal (Fig. 3*D*). The averaged time courses and time-lapsed functional maps revealed the reduced fMRI signal in the FP-S1 and the negative fMRI signal from the whole cortex upon the intrinsic astrocytic Ca^{2+} spiking events (Fig. 3 *E* and *F*). Furthermore, the intrinsic astrocytic Ca^{2+} spikes were also detected at different phases of the 30-s stimulation and the stimulation-off period (*SI Appendix*, Fig. S8 *A* and *B*). These results clearly demonstrated that two independent astrocytic Ca^{2+} signals (evoked vs. intrinsic) could concurrently occur with a unique combination of coexisting positive and negative BOLD signals in the brain.

Specifying the Spatiotemporal Features of the Intrinsic Astrocytic Ca^{2+} Spikes. Given that brain trauma may accompany the surgical procedure, we examined the possibility that the astrocytic Ca^{2+} signal is associated with spreading depolarization/depression (27). Astrocytic Ca^{2+} signals from two hemispheres in the 30-s stimulation block design were measured to determine whether the intrinsic astrocytic Ca^{2+} spike elicited by the stimulation traveled through the cortex. If the astrocytic Ca^{2+} spike was triggered from the activated FP-S1 due to the stimulation-induced spreading depolarization/depression, it should appear as a signal propagating through the cortex following stimulation (26, 28, 31). Fig. 4*A* shows that the intrinsic astrocytic Ca^{2+} spikes not only occurred in the activated FP-S1, but also were detected in FP-S1 of the opposite hemisphere despite the fact that no evoked astrocytic and fMRI signals were detected together with the negative BOLD signal through the cortex. The onset of the intrinsic astrocytic Ca^{2+} spike in activated FP-S1 during stimulation was measured by subtracting the normally evoked astrocytic Ca^{2+} spike to clearly display the overlapping onsets of the intrinsic astrocytic Ca^{2+} spikes detected from both hemispheres (Fig. 4*B*). The latencies of the intrinsic astrocytic Ca^{2+} spiking events in the two hemispheres varied from 2 to 4 s after the stimulus, but with little difference between them (Fig. 4*C*, *Left*, 2.29 ± 0.31 s vs. *Right*, 2.42 ± 0.12 s, paired t test, $P = 0.26$; CI values in *SI Appendix*, Table S2). Periodically, the intrinsic astrocytic Ca^{2+} spike appeared at a later phase of the 30-s stimulation period and was detected in the other hemisphere with the same onset time (*SI Appendix*, Fig. S8 *C* and *D*).

This simultaneous appearance of the intrinsic astrocytic Ca^{2+} spikes in both hemispheres is inconsistent with previously reported astrocytic Ca^{2+} waves of spreading depression with propagation speed at ∼20–40 μm/s (31, 32, 38), as well as the astrocytic Ca^{2+}

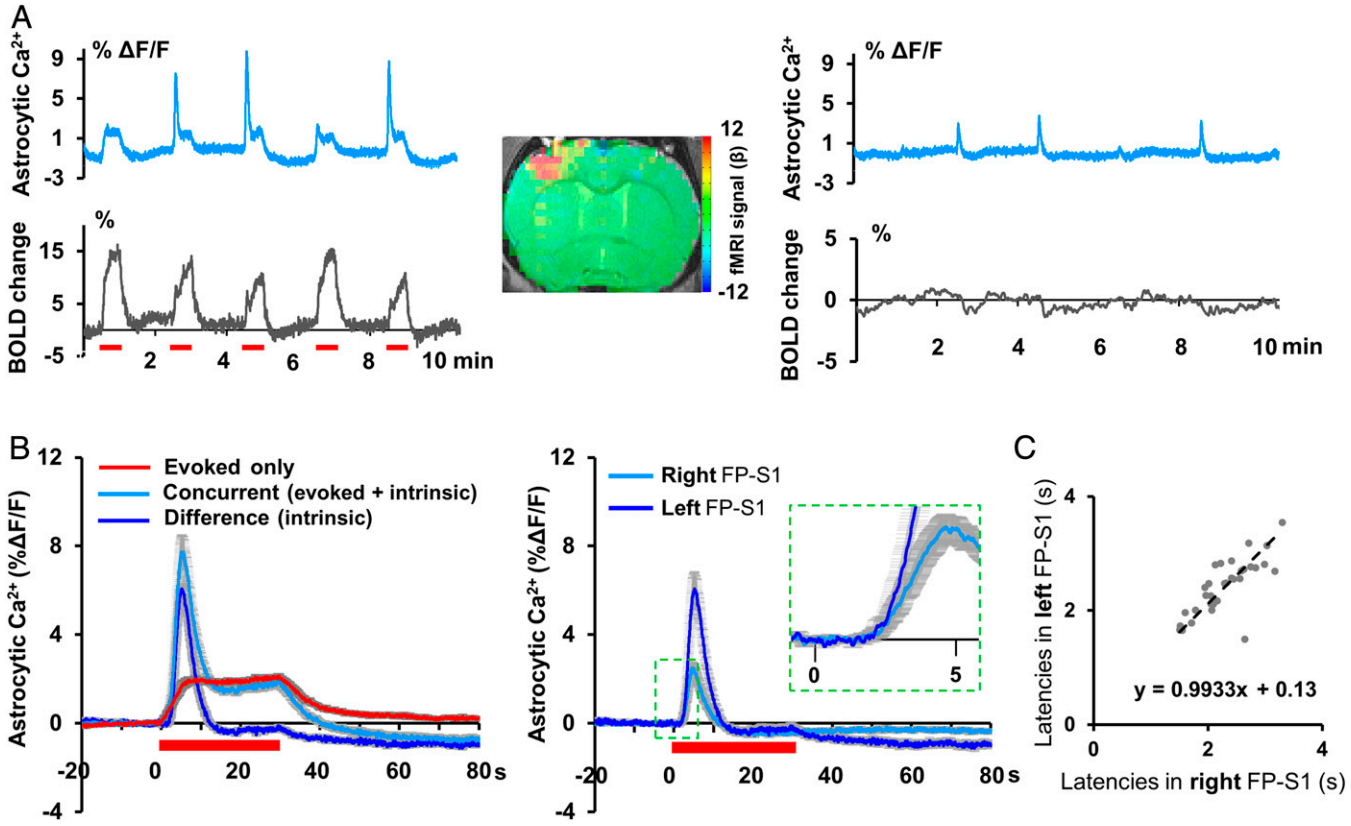

Fig. 4. Bilateral astrocytic Ca^{2+} recordings with simultaneous fMRI. (*A*) The representative traces of astrocytic Ca^{2+} and simultaneous BOLD signal in FP-S1 of both hemispheres with 30-s right forepaw stimulation (*Inset*: BOLD-fMRI map with left FP-S1 activation; concurrent events: epoch 2, 3, 5). (*B*) The mean time course of the astrocytic Ca^{2+} signal from evoked-only events vs. the concurrent (evoked + intrinsic) events (*Left*). The intrinsic astrocytic Ca^{2+} spike in the activated FP-S1 can be represented by subtracting the two events, which shows similar onset time to the intrinsic astrocytic Ca^{2+} spike detected in the opposite hemisphere (*Right*; mean ± SEM, rats, $n = 6$). *Inset* is a magnified figure of the dashed box. (*C*) The scatter plot of the latency estimated from the intrinsic astrocytic Ca^{2+} spikes of two hemispheres (Trial # = 32; rats, $n = 6$).

wave propagation detected in the hippocampus (60 μm/s) (30). The spreading depression events elicited Ca^{2+} signals at a higher intensity of electrical stimulation. Despite the high Ca^{2+} signal detected in both neurons and astrocytes upon the occurrence of spreading depression in the stimulated hemisphere, no Ca^{2+} signal was detected in the other hemisphere (*SI Appendix*, Fig. S9), consistent with a previous study showing that spreading depression is confined to the ipsilateral hemisphere with focal ischemia (29). This shows that the intrinsic astrocytic Ca^{2+} signal that mediates global neurovascular coupling in the cortex is independent of spreading depolarization/depression induced by brain lesions.

Using fMRI to Identify the Subcortical Functional Nuclei Correlated with the Intrinsic Astrocytic Ca^{2+} Signal. Subcortical nuclei that project throughout the entire neocortex could be responsible for the intrinsic astrocytic Ca^{2+}-mediated neurovascular coupling events. Based on the on/off stimulation block design, the neurovascular coupling events were separated into two groups: those in which only the evoked astrocytic Ca^{2+} signal was present in the activated cortex, i.e., evoked-only events, and those with concurrent evoked and intrinsic astrocytic Ca^{2+} signals, i.e., concurrent (evoked + intrinsic) bilateral events (Fig. 5*A*). The amplitudes of the astrocytic Ca^{2+} spike of the concurrent events were significantly higher than those of the evoked-only events (Fig. 3*C*) and were therefore also used to specify the two categories (Fig. 5*B*). The event-related fMRI analysis showed focal FP-S1 activation for the evoked events, but for the concurrent events, the amplitude of the BOLD signal in the FP-S1 was significantly reduced and a prolonged negative BOLD signal was detected throughout the cortex as well as in the subcortical regions (Fig. 5*C* and Movie S1). Interestingly, a positive BOLD signal was also detected in the central and mediodorsal thalamic nuclei at an early phase of the stimulation for concurrent events (Fig. 5 *B* and *C*). In addition, the subcortical activity pattern extended beyond the thalamus; particularly, from the central lateral and mediodorsal lateral thalamus to the midbrain reticular formation (Fig. 5*D*, brain atlas overlapped; *SI Appendix*, Fig. S10, multislice functional map; Movie S2, 3D rendering video). Simultaneous recording of fMRI and Ca^{2+} signals can therefore be used to locate specific functional nuclei underlying unique neurovascular coupling on a whole-brain scale.

To confirm the thalamic BOLD activation during concurrent events, the LFP in the central thalamic region was recorded simultaneously with the astrocytic Ca^{2+} recording in the cortex. The central lateral (CL) thalamic regions were specifically targeted based on the BOLD functional map with the concurrent events, showing bilateral activation pattern covering a region of the brain atlas 400–500 μm in extant (Fig. 5*D*). For precise localization, the position of the electrode tip for each experiment was imaged by MRI (*SI Appendix*, Fig. S11). Fig. 6*A* shows the power spectral density of the LFP signal recorded from both the central thalamic region and the FP-S1, as well as the astrocytic Ca^{2+} signal detected in the FP-S1 in response to electrical stimulation of the forepaw. Interestingly, an elevated spectral power level was detected in both the thalamus and cortex before the induction of the intrinsic astrocytic Ca^{2+} spike from the on/off stimulation trial, followed by reduced power levels. A similar phenomenon was shown by the two-channel bilateral Ca^{2+} recording

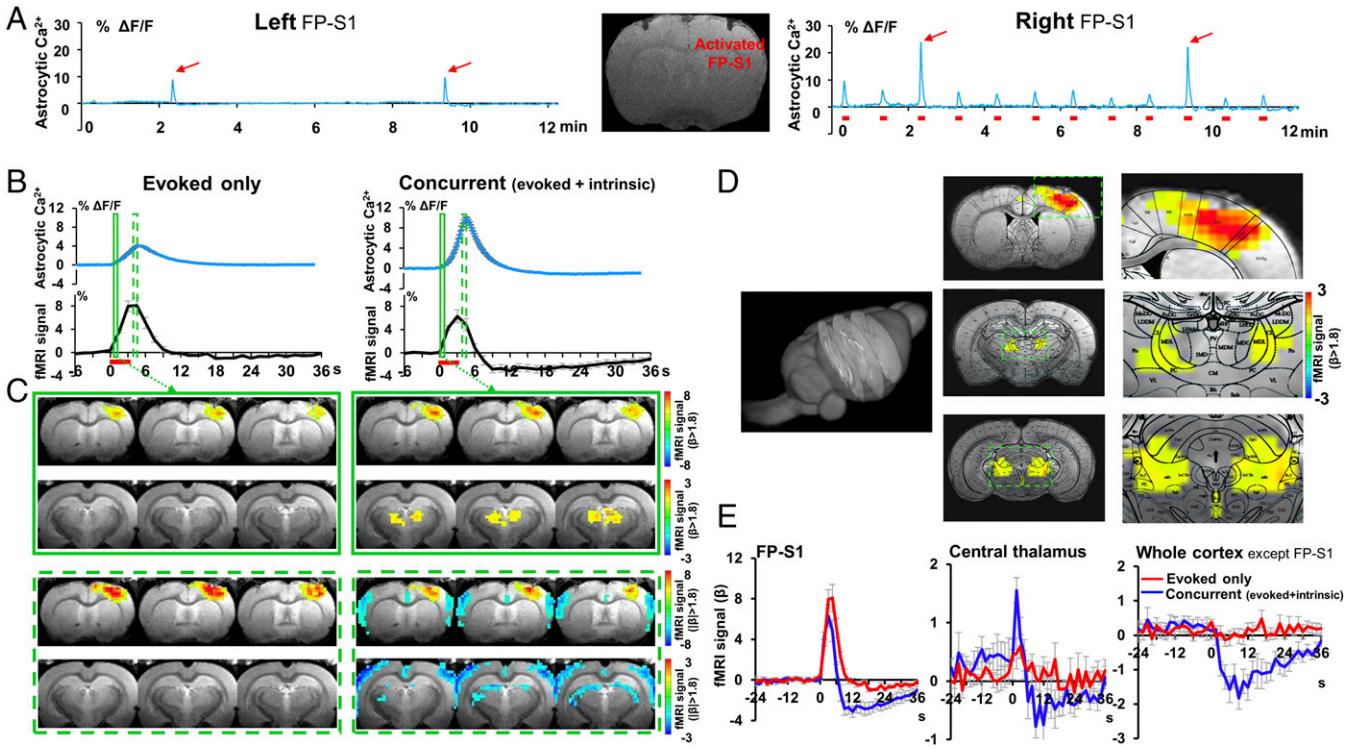

Fig. 5. Subcortical fMRI activation patterns underlying the intrinsic astrocytic Ca^{2+} spikes. (*A*) The representative traces of the FP-S1 astrocytic Ca^{2+} signals in both hemispheres (Right FP-S1 activation, 12 epochs, 3 Hz, 4 s, 1.5 mA; *Inset*, fiber traces in the anatomical MRI image; concurrent events, epoch 3 and 10, red arrows). (*B*) The averaged astrocytic Ca^{2+} and simultaneous fMRI signal of the evoked-only and concurrent events. (*C*) The time-lapsed function maps at 1.5 s (solid green box) and 4.5 s (dashed green box) after onset of stimulation (*Left*: evoked-only FP-S1 activation; *Right*: concurrent events, thalamic activation at 1.5 s, followed by the negative fMRI signal in the cortex and ventricle areas at 4.5 s). (*D*) The concurrent event functional maps at 1.5 s were overlapped on three anatomic slices characterized from a 3D whole brain and the corresponding brain atlas (*Right*: the enlarged images with activity patterns on the FP-S1, central thalamus, and the midbrain reticular formation region). (*E*) The time course of the BOLD fMRI signal from FP-S1, central thalamic region, and the whole cortex except FP-S1 (trial # = 72; rats: n = 6, mean ± SEM).

setup (left FP-S1, neuronal Ca^{2+} vs. right FP-S1, astrocytic Ca^{2+}). An increased EEG-like power level of neuronal Ca^{2+} transients was detected before the intrinsic astrocytic Ca^{2+} events upon electrical stimulation, followed by reduced power levels as well (*SI Appendix*, Fig. S12). These results indicate that the intrinsic astrocytic Ca^{2+} events may rely on the brain state fluctuation.

The event-related analysis scheme used previously was applied to acquire the mean power spectral density of the LFP signal based on the evoked-only events and concurrent events of the simultaneously recorded astrocytic Ca^{2+} signal (Fig. 6 *B* and *C*). The power levels in different EEG frequency bands before and after the stimulation in the evoked-only events indicated no difference between recordings from the thalamus and cortex (Fig. 6 *B* and *C*). In contrast, for the concurrent events, a higher EEG power level occurred before the onset of stimulation and a short transient in the EEG power spectrum was detected at frequencies up to 40 Hz upon stimulation (Fig. 6*B*). Quantitative analysis of the different EEG frequency bands in both the thalamus and cortex showed no detectable difference between both events in the delta band (1–4 Hz). For concurrent events, both the theta (4–8 Hz) and alpha band (8–13 Hz) power levels were significantly higher before stimulation than in evoked-only events (Fig. 6*C*, nonoverlapping CIs; *SI Appendix*, Table S2). Similar patterns were also shown in the EEG-like power spectral analysis for the simultaneously acquired neuronal Ca^{2+} signal (*SI Appendix*, Fig. S12). Also noteworthy is that the beta band (13–30 Hz) power level increased upon stimulation and was significantly higher than during the evoked events, which could contribute to the positive BOLD signal detected only in the concurrent events (Fig. 6*B*). The increased power in the beta frequency band in the thalamus may be attributable to a desynchronized arousal fluctuation that may shift the cortex to more alert brain states and underlie the intrinsic astrocytic Ca^{2+}-mediated neurovascular coupling events.

Discussion

Simultaneously recorded fMRI and GCaMP-mediated Ca^{2+} signals were used to characterize the cell-specific neurovascular coupling events underlying two types of fMRI signals in anesthetized rats. In addition to the conventionally evoked BOLD fMRI signal positively correlated to the neuronal and astrocytic Ca^{2+} signal, an intrinsic astrocytic Ca^{2+} spike was observed that showed unique spatiotemporal features in the cortex and was accompanied by reduced power levels in the EEG across a broad range of frequencies and a negative BOLD signal throughout the cortex. Periodically, the intrinsic and evoked astrocytic Ca^{2+} signals occurred concurrently with neurovascular coupling events at opposite signs, demonstrating that two distinct gliovascular effects on vessel constriction and dilation can occur in vivo under the same conditions. Furthermore, both fMRI brain mapping and LFP recording revealed that increased activity in the thalamic nuclei preceded the intrinsic astrocytic Ca^{2+} signal followed by the negative BOLD signal throughout the cortex. This suggests that the astrocyte-coupled bidirectional fMRI signal originates from thalamic regulation of brain state changes, which may be related to the anticorrelated thalamic and cortical fMRI signals observed during fluctuations in the state of arousal (15).

Previous studies of simultaneous fMRI and electrophysiology have demonstrated that the positive BOLD signal is correlated with increased neuronal activity, and that the negative BOLD

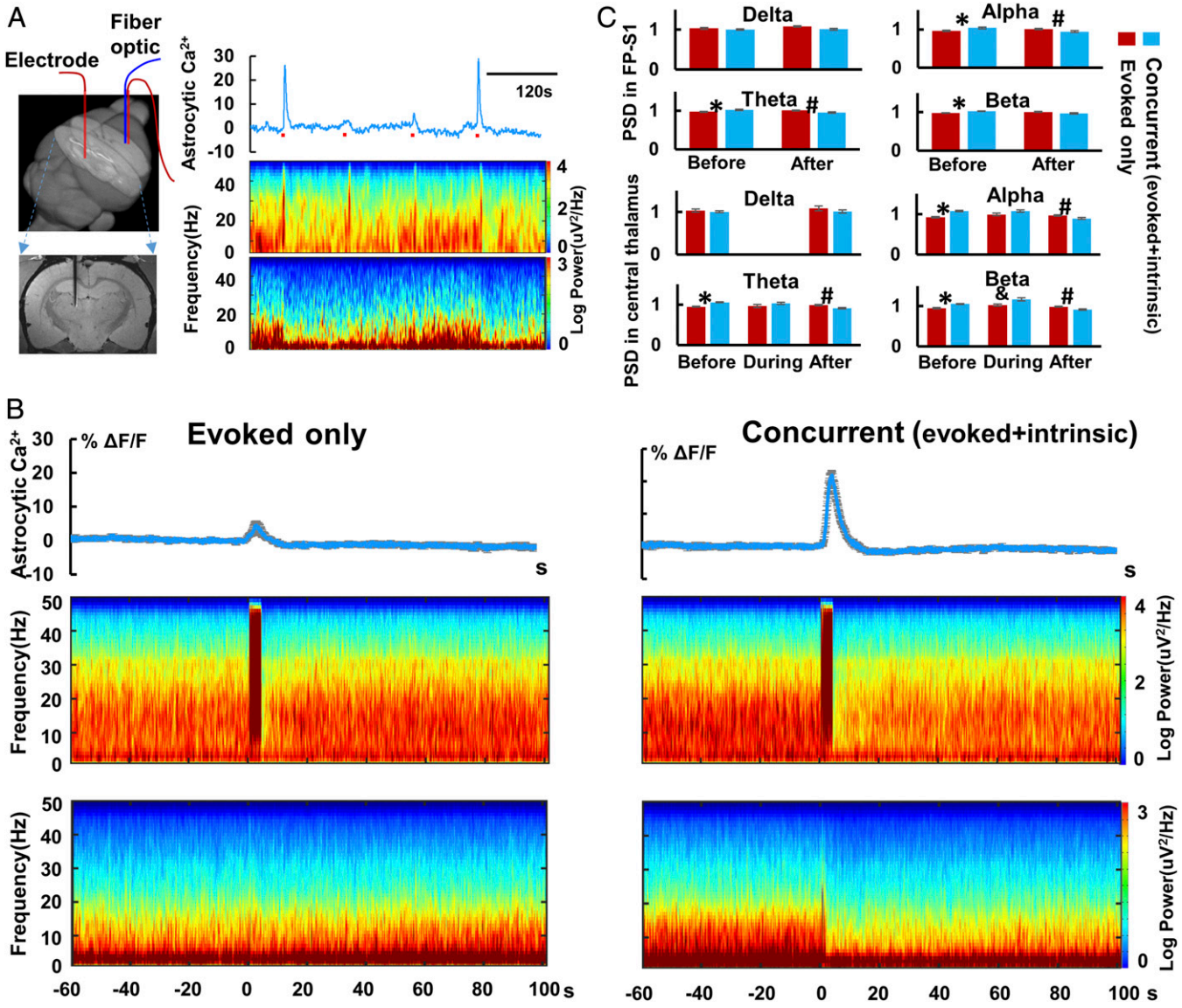

Fig. 6. Simultaneous astrocytic Ca^{2+} recording and the LFP recordings in both central thalamus and FP-S1. (*A*) The representative trace of the FP-S1 astrocytic Ca^{2+} signal (*Top Right*), the LFP power spectrogram in FP-S1 (*Middle Right*) and the contralateral central thalamus (*Bottom Right*) with forepaw electrical stimulation (3 Hz, 4 s, 1.5 mA; *Inset*, 2D slices with electrode insertion in the central thalamic region). (*B*) Evoked-only and concurrent events were separated to show the averaged astrocytic Ca^{2+} signal and LFP power spectrogram (1-s sliding window with 0.1-s steps, 9 tapers). (*C*) The normalized mean spectral power of different EEG bands (evoked-only, red, trial # = 98; concurrent, blue, trial # = 57, rats, $n = 4$) at different phases of the stimulation on/off trials (before: −40 to −20 s; during: 0–1.5 s; and after: 60–80 s; FP-S1: theta, $*P = 1.5e\text{-}05$, $\#P = 0.012$; alpha, $*P = 1.3e\text{-}07$, $\#P = 0.019$; beta, $*P = 1.6e\text{-}07$; central thalamic region: theta, $*P = 0.00018$, #, $P = 0.0025$; alpha, $*P = 3.3e\text{-}05$, #, $P = 0.0068$; beta, $*P = 0.00010$, &$P = 0.0022$, $\#P = 0.0025$; mean ± SEM; delta power was calculated from 4-s windows in 0.1-s steps).

signal from the surrounding cortical area is associated with decreased neuronal activity (2, 39). It has also been established that the BOLD fMRI signal is directly linked to the hemodynamic signal coupled to the blood flow changes mediated by vascular activity, but the detailed neurovascular coupling events contributing to the bidirectional fMRI signal changes remain unclear (1). Earlier studies have shown that the astrocytic Ca^{2+} signal plays a crucial role in controlling blood flow through gliovascular interaction (3, 4) and especially vasoconstriction and vasodilation under a variety of conditions (7, 8, 12, 40). Upon sensory stimulation, increased neuronal activity (both LFP and neuronal Ca^{2+} signals) is correlated with the evoked astrocytic Ca^{2+} in vivo signal as well as the BOLD fMRI signal, enabling the direct measurement of the fMRI signal with the underlying neuron–glia–vascular interaction (Fig. 1). Optical fiber was used to record the Ca^{2+} signal from astrocytes in deep cortical layers, in contrast to the previous in vivo optical measurement from superficial layers of the cortex (5, 10, 19, 41), enabling the detection of the Ca^{2+} signal from a population of astrocytes located in layer 5 of the cortex. The optical fiber integrated the Ca^{2+} signal from both astrocytic soma and processes directly coupled to pyramidal neurons located at layer 5, which could account for the 1- to 1.7-s latency of the evoked astrocytic Ca^{2+} signal, which is shorter than reported in previous studies (5, 10). Several other optical imaging studies have also reported the rapid onset of evoked Ca^{2+} signal in astrocytes in vivo (11, 35), as well as fast miniature Ca^{2+} transients in the hippocampal slice (42), indicating that the evoked astrocytic signal may be involved in neurovascular coupled vessel dilation underlying the positive BOLD fMRI signal. It is noteworthy that the activity-coupled

vasodilation persists in mice with IP3-2 receptor knock-out ($IP3R2^{-/-}$) to inhibit the astrocytic Ca^{2+} intracellular release, therefore indicating that there may be a parallel pathway to mediate the astrocytic Ca^{2+}-independent vasodilation (5, 43). Interestingly, a recent study reported the astrocytic calcium fluctuation in $IP3R2^{-/-}$ mice upon startle responses (44). In contrast, the capillary dilation could be controlled by glial Ca^{2+} signal (43). In $IP3R2^{-/-}$ mice, the capillary dilation is abolished where the glial Ca^{2+} signal is reduced (6). This study suggests that the astrocytic Ca^{2+} signal may mediate the neurovascular coupling through capillary control. In addition, the causal relationship of the astrocytic Ca^{2+} signal with BOLD fMRI can be further specified in transgenic mice with inhibited astrocytic Ca^{2+} intracellular release and pericyte-deficient mice (5, 45).

Astrocytic Ca^{2+}-mediated vessel constriction has been observed in vivo under spreading suppression (31). Similarly, the death of pericytes in the ischemic brain also causes capillary constriction in vivo (46). It remains to be determined whether the elevated astrocytic Ca^{2+} causes negative BOLD signal changes through vasoconstriction during normal functioning. Here, we showed that the intrinsic astrocytic Ca^{2+} spike was the crucial linkage of neurovascular coupling to mediate the negative BOLD signal in the whole cortex. The data show that the intrinsic astrocytic Ca^{2+} spike is accompanied by decreased high frequency (3–40 Hz) power of the spontaneous LFP signal with a slight lag, consistent with two-photon imaging studies in mice anesthetized with urethane (9). The absence of slow-frequency oscillations in the present study could be due to anesthetics and differences with α-chloralose (36, 47). Interestingly, in the hippocampus of mice anesthetized with urethane, astrocytic Ca^{2+} waves have been reported to correlate with the decreased power level in both infraslow and high-frequency ranges, as well as with reduced blood flow (30). Besides the spontaneous neuronal oscillation, the astrocytic Ca^{2+} transients have also been reported to be coupled with carbachol-induced oscillations in the hippocampal brain slices (34). Therefore, the intrinsic astrocytic Ca^{2+}-coupled negative BOLD signal may represent one of the multiple ways that astrocytes affect neurovascular coupling and modulate brain states (7).

What is the relationship between spreading depression of the lesioned brain and the intrinsic astrocytic Ca^{2+} signal with decreased BOLD signal? Spreading depolarization/depression can be elicited by numerous noxious triggers, such as chemical treatment with potassium and glutamate, hypoxia, and focal ischemia, as well as in the healthy intact cortex (26, 27). The persistent depression of activity and reduction of blood flow usually follows spreading depolarization in the cortex, which is also accompanied with Ca^{2+} waves propagating through the local neuronal and astrocytic network from the triggered source (28, 48, 49). However, the novel intrinsic astrocytic Ca^{2+}-mediated neurovascular coupling events showed spatiotemporal features distinct from spreading depression (*SI Appendix*, Fig. S8). First, intrinsic astrocytic Ca^{2+} signals can occur concurrently with the evoked astrocytic Ca^{2+} signal, mediating, respectively, both positive and negative BOLD fMRI signals in the brain. Although the elevated astrocytic Ca^{2+} leads to the secretion of different vasoactive agents, such as prostaglandin E2, epoxyeicosatrienoic acids, and 20-HETE, under different conditions (7, 8, 12, 37), the large-scale astrocytic Ca^{2+}-mediated vasoconstriction that is usually detected in the pathological conditions of the cortex is not accompanied by simultaneous positive events in vivo (31). Second, there was no propagation delay of the intrinsic astrocytic Ca^{2+} spikes in the two hemispheres (Fig. 4), which is different from Ca^{2+} waves traveling through the astrocytic network from the source of spreading depression (31, 32). We presented evidence that the intrinsic astrocytic Ca^{2+} signals detected instantaneously throughout the cortex (Figs. 3 and 4) were initiated by subcortical projections activating the intrinsic astrocytic Ca^{2+}-mediated neurovascular coupling events (50, 51).

The intrinsic astrocytic Ca^{2+} signal mediates the regulation of brain states through the reticular formation ascending pathway, which is known to regulate arousal (52). Although initiated in the anesthetized rat brain, the intrinsic astrocytic Ca^{2+}-mediated neuronal activity changes may shed light on the thalamic regulation of the state switch leading to arousal. The simultaneously acquired astrocytic Ca^{2+} signal led to the identification of the activated thalamic and midbrain reticular formation regions in fMRI brain mapping based on the occurrence of the intrinsic astrocytic Ca^{2+} spikes (Figs. 5 and 6, *SI Appendix*, Fig. S10, and Movie S2). Two striking features were detected: First, positive BOLD signals were detected in the thalamic regions in contrast to negative BOLD signals detected throughout the entire cortex. These results are consistent with the fMRI activity pattern reported in a recent resting-state fMRI study, showing that increased fMRI signals in the thalamus and decreased fMRI signals in the whole cortex are correlated with state fluctuation associated with arousal at eye opening (15). Optogenetic activation of the central lateral thalamus at low frequency also initiates the negative BOLD signal across the whole cortex of the anesthetized rat brain (53). Second, the increased alpha power in both the thalamus and cortex was detected before the occurrence of the intrinsic astrocytic spike, which was then followed by decreased alpha power. This could provide insights into what cortical states predispose toward the induction of these Ca^{2+} spikes. Alpha power is also reduced following eye opening (54). The regulation of alpha-power oscillation-dependent brain states is less efficient when delivered upon the high alpha-power state (55, 56). It is plausible that the intrinsic astrocytic Ca^{2+} spikes may be involved in the spontaneous fluctuation of the alpha-band EEG activity to mediate the brain excitability (56).

Two issues remain to be solved to better understand the interaction of astrocytic calcium and BOLD fMRI signal during the brain state fluctuation. The first issue is the brain state dependency and potential anesthetic effects on the correlation of astrocytic calcium signal and BOLD fMRI signal. Besides α-chloralose, the negative BOLD signal coupled to the intrinsic astrocytic Ca^{2+} spikes was observed in rats anesthetized with urethane (*SI Appendix*, Fig. S13). This result demonstrates that the negative correlation is not just caused by the α-chloralose anesthetic effect. Interestingly, the negative BOLD correlation pattern varied across different animals, indicating a potential dependency on the anesthetic effect of urethane (*SI Appendix*, Fig. S14). In a preliminary experiment, the astrocytic Ca^{2+} signal was recorded simultaneously with LFP in free-moving rats, showing the intrinsic astrocytic Ca^{2+} spikes in coincidence with the EEG state changes during sleep cycles (*SI Appendix*, Fig. S15). This preliminary result further implicates the highly correlated intrinsic astrocytic Ca^{2+} signals with brain state changes, similar to what has been reported in the urethane-anesthetized rats (9).

The second issue is to clarify the causal relationship of the intrinsic astrocytic Ca^{2+} signal to the negative BOLD signal and their underlying molecular mechanism. In the present study, both intrinsic astrocytic Ca^{2+} signal and negative BOLD signal were dampened in rats anesthetized with medetomidine, an adrenergic alpha-2 receptor agonist, which can inhibit norepinephrine effect through negative feedback (*SI Appendix*, Fig. S16). It has been shown that the locomotion- or startle-induced astrocytic Ca^{2+} signal can be blocked by trazodone or prazosin, the inhibitor or antagonist of adrenergic receptors, and abolished by neurotoxin DSP4 with local norepinephrine depletion (57, 58). These results indicate that the noradrenergic system may mediate both intrinsic astrocytic Ca^{2+} signal and vasoconstriction, respectively or sequentially (59). It is also possible that the

central thalamic nuclei and the midbrain reticular formation are directly mediated by the norepinephrine projections or are coactivated to elicit the intrinsic astrocytic Ca^{2+} signal and the negative BOLD signal in the whole cortical area (60). Optogenetic activation of the locus coeruleus or central thalamic nulcei offers further prospects for studying the causal relationship and the direct norepinephrine-driven mechanism. The simultaneous astrocytic calcium recording with fMRI could be combined with optogenetic activation to specify the molecular and circuit mechanism underlying astrocyte-mediated gliovascular interaction and correlated brain state changes.

Materials and Methods

Detailed methods are provided in *SI Appendix*, *SI Materials and Methods*. The study was performed in accordance with the German Animal Welfare Act (TierSchG) and Animal Welfare Laboratory Animal Ordinance (TierSchVersV). This is in full compliance with the guidelines of the EU Directive on the protection of animals used for scientific purposes (2010/63/EU). The study was reviewed by the ethics commission (§15 TierSchG) and approved by the state authority (Regierungspräsidium, Tuebingen, Baden-Württemberg, Germany). A total of 88 Sprague–Dawley rats were used in this study.

Viral vectors were directly ordered and packaged from the University of Pennsylvania Vector Core: AAV5.Syn.GCaMP6f.WPRE.SV40 and AAV5.GfaABC1D.cyto-GCaMP6f.SV40 (Addgene52925; GfaABC1D.cyto promoter for cytoplasmic expression of GCaMP6f; ref. 61).

Similar procedures of fMRI animal preparation have been previously described (62). The two-channel optical setup for fiber-optic Ca^{2+} recordings has been developed base on a previous report (Fig. 1*C*) (19). The astrocytic calcium signal-dependent event-related fMRI analysis was applied to specify the subcortical brain activity patterns from the whole brain 3D-EPI fMRI images.

A paired Student's *t* test and one-way ANOVA were performed for statistical analysis. The data with error bars are mean ± SEM in each statistic graph. In addition, the mean and 95% CIs for the distribution of LFP power spectra density, estimated onset times, amplitude of the astrocytic Ca^{2+}, and BOLD signal were calculated using the bootstrap procedure (63). The 95% CIs are equivalent to hypothesis testing with a significance level of 0.05. Both confidence intervals with (nonoverlapping CIs) and *P* values for all statistical analysis were listed in *SI Appendix*, Table S2. Sample size was not previously estimated for the animal experiments, and no blinding and randomization design was needed in this work.

ACKNOWLEDGMENTS. We thank Dr. R. Pohmann, Dr. H. Merkle, Dr. K. Buckenmaier, Dr. Y. Jiang, Ms. P. Pais, and Ms. X. Chen for technical support; Ms. H. Schulz and S. Fischer for animal maintenance support; the Analysis of Functional NeuroImages (AFNI) team for the software support; and Dr. B. S. Khakh, the Genetically-Encoded Neuronal Indicator and Effector (GENIE) Program, and the Janelia Farm Research Campus for providing the astrocyte-specific promoter and GCaMP6 plasmids. This research was supported by German Research Foundation (DFG) SPP-1655, internal funding from Max Planck Society (to X.Y.), and HHMI support (to T.J.S.).

1. Attwell D, Iadecola C (2002) The neural basis of functional brain imaging signals. *Trends Neurosci* 25:621–625.
2. Logothetis NK, Pauls J, Augath M, Trinath T, Oeltermann A (2001) Neurophysiological investigation of the basis of the fMRI signal. *Nature* 412:150–157.
3. Attwell D, et al. (2010) Glial and neuronal control of brain blood flow. *Nature* 468: 232–243.
4. Petzold GC, Murthy VN (2011) Role of astrocytes in neurovascular coupling. *Neuron* 71:782–797.
5. Nizar K, et al. (2013) In vivo stimulus-induced vasodilation occurs without IP3 receptor activation and may precede astrocytic calcium increase. *J Neurosci* 33:8411–8422.
6. Biesecker KR, et al. (2016) Glial cell calcium signaling mediates capillary regulation of blood flow in the retina. *J Neurosci* 36:9435–9445.
7. Metea MR, Newman EA (2006) Glial cells dilate and constrict blood vessels: A mechanism of neurovascular coupling. *J Neurosci* 26:2862–2870.
8. Mulligan SJ, MacVicar BA (2004) Calcium transients in astrocyte endfeet cause cerebrovascular constrictions. *Nature* 431:195–199.
9. Poskanzer KE, Yuste R (2016) Astrocytes regulate cortical state switching in vivo. *Proc Natl Acad Sci USA* 113:E2675–E2684.
10. Wang X, et al. (2006) Astrocytic Ca2+ signaling evoked by sensory stimulation in vivo. *Nat Neurosci* 9:816–823.
11. Lind BL, Brazhe AR, Jessen SB, Tan FC, Lauritzen MJ (2013) Rapid stimulus-evoked astrocyte Ca2+ elevations and hemodynamic responses in mouse somatosensory cortex in vivo. *Proc Natl Acad Sci USA* 110:E4678–E4687.
12. Zonta M, et al. (2003) Neuron-to-astrocyte signaling is central to the dynamic control of brain microcirculation. *Nat Neurosci* 6:43–50.
13. Dombeck DA, Khabbaz AN, Collman F, Adelman TL, Tank DW (2007) Imaging large-scale neural activity with cellular resolution in awake, mobile mice. *Neuron* 56:43–57.
14. Sirotin YB, Das A (2009) Anticipatory haemodynamic signals in sensory cortex not predicted by local neuronal activity. *Nature* 457:475–479.
15. Chang C, et al. (2016) Tracking brain arousal fluctuations with fMRI. *Proc Natl Acad Sci USA* 113:4518–4523.
16. Logothetis NK, et al. (2012) Hippocampal-cortical interaction during periods of subcortical silence. *Nature* 491:547–553.
17. Girouard H, Iadecola C (2006) Neurovascular coupling in the normal brain and in hypertension, stroke, and Alzheimer disease. *J Appl Physiol (1985)* 100:328–335.
18. Akerboom J, et al. (2013) Genetically encoded calcium indicators for multi-color neural activity imaging and combination with optogenetics. *Front Mol Neurosci* 6:2.
19. Schulz K, et al. (2012) Simultaneous BOLD fMRI and fiber-optic calcium recording in rat neocortex. *Nat Methods* 9:597–602.
20. Chen TW, et al. (2013) Ultrasensitive fluorescent proteins for imaging neuronal activity. *Nature* 499:295–300.
21. Adelsberger H, Garaschuk O, Konnerth A (2005) Cortical calcium waves in resting newborn mice. *Nat Neurosci* 8:988–990.
22. Lütcke H, et al. (2010) Optical recording of neuronal activity with a genetically-encoded calcium indicator in anesthetized and freely moving mice. *Front Neural Circuits* 4:9.
23. Sanganahalli BG, et al. (2016) Comparison of glomerular activity patterns by fMRI and wide-field calcium imaging: Implications for principles underlying odor mapping. *Neuroimage* 126:208–218.
24. Adelsberger H, Zainos A, Alvarez M, Romo R, Konnerth A (2014) Local domains of motor cortical activity revealed by fiber-optic calcium recordings in behaving non-human primates. *Proc Natl Acad Sci USA* 111:463–468.
25. Kim CK, et al. (2016) Simultaneous fast measurement of circuit dynamics at multiple sites across the mammalian brain. *Nat Methods* 13:325–328.
26. Dreier JP (2011) The role of spreading depression, spreading depolarization and spreading ischemia in neurological disease. *Nat Med* 17:439–447.
27. Ayata C, Lauritzen M (2015) Spreading depression, spreading depolarizations, and the cerebral vasculature. *Physiol Rev* 95:953–993.
28. Nedergaard M, Cooper AJL, Goldman SA (1995) Gap junctions are required for the propagation of spreading depression. *J Neurobiol* 28:433–444.
29. Nedergaard M, Hansen AJ (1993) Characterization of cortical depolarizations evoked in focal cerebral ischemia. *J Cereb Blood Flow Metab* 13:568–574.
30. Kuga N, Sasaki T, Takahara Y, Matsuki N, Ikegaya Y (2011) Large-scale calcium waves traveling through astrocytic networks in vivo. *J Neurosci* 31:2607–2614.
31. Chuquet J, Hollender L, Nimchinsky EA (2007) High-resolution in vivo imaging of the neurovascular unit during spreading depression. *J Neurosci* 27:4036–4044.
32. Peters O, Schipke CG, Hashimoto Y, Kettenmann H (2003) Different mechanisms promote astrocyte Ca2+ waves and spreading depression in the mouse neocortex. *J Neurosci* 23:9888–9896.
33. Poskanzer KE, Yuste R (2011) Astrocytic regulation of cortical UP states. *Proc Natl Acad Sci USA* 108:18453–18458.
34. Lee HS, et al. (2014) Astrocytes contribute to gamma oscillations and recognition memory. *Proc Natl Acad Sci USA* 111:E3343–E3352.
35. Winship IR, Plaa N, Murphy TH (2007) Rapid astrocyte calcium signals correlate with neuronal activity and onset of the hemodynamic response in vivo. *J Neurosci* 27: 6268–6272.
36. Winters WD, Spooner CE (1966) A neurophysiological comparison of alpha-chloralose with gamma-hydroxybutyrate in cats. *Electroencephalogr Clin Neurophysiol* 20: 83–90.
37. Gordon GRJ, Choi HB, Rungta RL, Ellis-Davies GCR, MacVicar BA (2008) Brain metabolism dictates the polarity of astrocyte control over arterioles. *Nature* 456: 745–749.
38. Kuchibhotla KV, Lattarulo CR, Hyman BT, Bacskai BJ (2009) Synchronous hyperactivity and intercellular calcium waves in astrocytes in Alzheimer mice. *Science* 323: 1211–1215.
39. Shmuel A, Augath M, Oeltermann A, Logothetis NK (2006) Negative functional MRI response correlates with decreases in neuronal activity in monkey visual area V1. *Nat Neurosci* 9:569–577.
40. Devor A, et al. (2007) Suppressed neuronal activity and concurrent arteriolar vasoconstriction may explain negative blood oxygenation level-dependent signal. *J Neurosci* 27:4452–4459.
41. Srinivasan R, et al. (2016) New transgenic mouse lines for selectively targeting astrocytes and studying calcium signals in astrocyte processes in situ and in Vivo. *Neuron* 92:1181–1195.
42. Di Castro MA, et al. (2011) Local Ca2+ detection and modulation of synaptic release by astrocytes. *Nat Neurosci* 14:1276–1284.
43. Mishra A, et al. (2016) Astrocytes mediate neurovascular signaling to capillary pericytes but not to arterioles. *Nat Neurosci* 19:1619–1627.
44. Srinivasan R, et al. (2015) Ca(2+) signaling in astrocytes from Ip3r2(-/-) mice in brain slices and during startle responses in vivo. *Nat Neurosci* 18:708–717.
45. Armulik A, et al. (2010) Pericytes regulate the blood-brain barrier. *Nature* 468: 557–561.
46. Hall CN, et al. (2014) Capillary pericytes regulate cerebral blood flow in health and disease. *Nature* 508:55–60.

47. Steriade M, Nuñez A, Amzica F (1993) A novel slow (< 1 Hz) oscillation of neocortical neurons in vivo: Depolarizing and hyperpolarizing components. *J Neurosci* 13: 3252–3265.
48. Nedergaard M (1994) Direct signaling from astrocytes to neurons in cultures of mammalian brain cells. *Science* 263:1768–1771.
49. Parpura V, et al. (1994) Glutamate-mediated astrocyte-neuron signalling. *Nature* 369: 744–747.
50. Hamel E (2006) Perivascular nerves and the regulation of cerebrovascular tone. *J Appl Physiol (1985)* 100:1059–1064.
51. Cauli B, et al. (2004) Cortical GABA interneurons in neurovascular coupling: Relays for subcortical vasoactive pathways. *J Neurosci* 24:8940–8949.
52. Edlow BL, et al. (2012) Neuroanatomic connectivity of the human ascending arousal system critical to consciousness and its disorders. *J Neuropathol Exp Neurol* 71:531–546.
53. Liu J, et al. (2015) Frequency-selective control of cortical and subcortical networks by central thalamus. *eLife* 4:e09215.
54. Berger H (1929) Über das Elektrenkephalogramm des Menschen. *Arch Psychiatr Nervenkr* 87:527–570.
55. Silvanto J, Muggleton N, Walsh V (2008) State-dependency in brain stimulation studies of perception and cognition. *Trends Cogn Sci* 12:447–454.
56. Romei V, et al. (2008) Spontaneous fluctuations in posterior alpha-band EEG activity reflect variability in excitability of human visual areas. *Cereb Cortex* 18:2010–2018.
57. Ding F, et al. (2013) α1-Adrenergic receptors mediate coordinated Ca2+ signaling of cortical astrocytes in awake, behaving mice. *Cell Calcium* 54:387–394.
58. Paukert M, et al. (2014) Norepinephrine controls astroglial responsiveness to local circuit activity. *Neuron* 82:1263–1270.
59. O'Donnell J, Ding F, Nedergaard M (2015) Distinct functional states of astrocytes during sleep and wakefulness: Is norepinephrine the master regulator? *Curr Sleep Med Rep* 1:1–8.
60. Carter ME, et al. (2010) Tuning arousal with optogenetic modulation of locus coeruleus neurons. *Nat Neurosci* 13:1526–1533.
61. Shigetomi E, et al. (2013) Imaging calcium microdomains within entire astrocyte territories and endfeet with GCaMPs expressed using adeno-associated viruses. *J Gen Physiol* 141:633–647.
62. Yu X, et al. (2016) Sensory and optogenetically driven single-vessel fMRI. *Nat Methods* 13:337–340.
63. Van Dort CJ, et al. (2015) Optogenetic activation of cholinergic neurons in the PPT or LDT induces REM sleep. *Proc Natl Acad Sci USA* 112:584–589.